

Self-lensing of moving gravitational-wave sources can break the microlensing crossing timescale degeneracy

Helena Ubach ^{1, 2, *}

¹*Departament de Física Quàntica i Astrofísica (FQA),
Universitat de Barcelona (UB), c. Martí i Franquès, 1, 08028 Barcelona, Spain*

²*Institut de Ciències del Cosmos (ICCUB), Universitat de Barcelona (UB),
c. Martí i Franquès, 1, 08028 Barcelona, Spain*

When a moving gravitational-wave (GW) source travels behind a massive astrophysical object, its signal is gravitationally lensed, showing a waveform distortion similar to a Paczyński curve. We present a first study of the lensing signature of a massive black hole (MBH) on a frequency-dependent GW signal from a moving binary merger. For both light and GW sources in a Keplerian circular orbit around a MBH lens, the self-lensing geometry breaks the microlensing degeneracy in the Einstein radius crossing timescale t_E . The duration of the curve ($2t_E$) becomes independent on the MBH mass M_{MBH} , and provides a direct measure of the distance d_{LS} to the MBH. However, M_{MBH} remains unknown. We show that, in GW signals, the redshifted mass $M_{\text{MBH},z}$ can additionally be obtained from the interference pattern, by measuring the modulation period T , the GW frequency f , and t_E : $M_{\text{MBH},z} \simeq 2.5 \times 10^6 M_{\odot} (t_E/[100 \text{ s}]) (f T)^{-1}$. If this lensing signature is not considered, it may be confused with other waveform distortions, especially in the modeling of overlapping signals in next generation ground-based GW detectors. The observation of one of these curves and its associated parameters may help (1) constrain the orbital distance d_{LS} of sources, especially around low mass MBHs at the centers of star clusters and galaxies, (2) additionally estimate the mass $M_{\text{MBH},z}$ of these MBHs, and (3) infer the orbital inclination of the binary. Simultaneously obtaining d_{LS} and $M_{\text{MBH},z}$ through self-lensing can help constrain the astrophysical environments where GW signals come from.

I. INTRODUCTION

When light and gravitational waves (GWs) travel through the space-time curvature of massive astrophysical objects, they are deflected and distorted by gravitational lensing. Lensing effects have been detected with light [1–3], although they have not confidently been detected with GWs yet [4–8] (though see [9]). GWs from binary mergers, usually referred to as compact binary coalescences (CBCs), have been detected by ground based detectors from the LIGO-Virgo-KAGRA (LVK) Collaboration. To date, nearly 300 GW events have been confidently detected [10–15]. As the number of GW events from CBCs increases, the lensing effect is expected to be detected on GWs soon [16–21].

The approaches to the observation of lensing of light and lensing of GWs are generally different, due to the nature of the detection methods. For light, lensing effects appear as either (1) multiple images of the same source, resolved through imaging (strong lensing); (2) transient increase of the source brightness following a Paczyński curve [22], when the source temporarily travels behind the lens, seen through photometry (microlensing); (3) astrometric microlensing. For transient GWs detectable in ground-based detectors, the equivalent of strong lensing is the detection of multiple images of a static source in time domain. Given the transient nature of the detected compact binary merger (CBC) sources, the equivalent to microlensing by low mass lenses is probed through wave

optics distortions for static sources [23, 24], rather than moving sources. The equivalent of the Paczyński curve is usually not considered for transient GWs from CBCs in ground-based detectors. Studies either consider a static source and varying frequency [e.g., 25–28] or a constant frequency and a moving source, the latter of which has been analyzed for continuous GW sources [e.g., 29–33]. Joint studies have been done for space-based detectors [34, 35]. To the best of the author’s knowledge, no previous studies have been done for a frequency-dependent moving source in ground-based detectors.

The frequency-dependent moving GW source is a case that can already be detectable in LVK. It may become especially relevant for future ground-based detectors such as Einstein Telescope (ET) and Cosmic Explorer (CE), when the signals are expected to last up to \sim hours in the initial inspiral phase of a binary merger. The lensing signature of the moving source — a Paczyński-like curve — on the CBC GW signal may reach a comparable amplitude to the merger phase. This transient modification of the signal could lead to misinterpretations if this effect is not taken into account, especially when treating overlapping signals.

The observation of the lensing curve can give us information of the parameters of the lensing system. In microlensing of light, the duration of the curve (twice the Einstein crossing timescale t_E) usually has a degeneracy between the lens mass, a combination of the distances, and the relative velocity of the lens and the source. The degeneracy may be broken by measuring the parallax [36–38], simultaneous parameters [39, 40, for a review], finite-source effects [41, 42], or relativistic effects [43]. By

* helenaubach@icc.ub.edu

contrast, when the source is orbiting a massive black hole (MBH) that acts as the lens (*self-lensing*), the Einstein crossing timescale is only dependent on the orbital distance d_{LS} from the source to the lens [44]. For both light and GWs, the breaking of the Einstein crossing timescale degeneracy thus provides an independent way to measure the orbital distance d_{LS} of the source.

Gravitational waves offer an additional opportunity to extract more parameters from the signal: their coherence and long wavelengths produce wave optics effects, such as interference between the multiple images. The modulation of the signal by the interference pattern makes it possible to measure the redshifted mass of the MBH $M_{\text{MBH},z}$ from the period of these modulations, the frequency of the GWs, and the crossing timescale t_E .

The combination of these capabilities for GW sources provides a way to potentially infer the distance d_{LS} and the mass $M_{\text{MBH},z}$ simultaneously. The observation of these lensing curves and their associated orbital parameters may help constrain the distance distribution of CBCs, especially around low mass MBHs. It can also help disentangle scaling degeneracies between the orbital distance and the MBH mass which otherwise require the simultaneous measurement of the velocity and the acceleration of the source [45].

In this work, we obtain the lensing signature on a GW signal “chirp” from a quasi-circular CBC (Sec. II). We then analyze how to extract the orbital distance d_{LS} (Sec. III), the MBH mass $M_{\text{MBH},z}$ (Sec. IV) and potentially the inclination of the binary (Sec. V) from the signal features. We finally discuss the limitations of this study and future directions.

II. LENSING CURVE ON A CHIRPING SIGNAL

The astrophysical configuration considered in this work is shown in Fig. 1: a compact binary at S orbits a massive black hole (MBH) at L, at an orbital distance d_{LS} . The compact binary is a source of GWs and results in a CBC. When it travels behind the MBH, the emitted GWs undergo gravitational lensing by the MBH lens. When the binary is bound to the MBH’s potential, we refer to the case as *self-lensing* [46], and the velocity of the source corresponds to the orbital velocity v_{orb} .

The source travels behind the lensing cross-section, generally¹ given by πR_E^2 , where R_E is the Einstein radius, which for self-lensing is simplified to $R_E \simeq \sqrt{2R_S d_{LS}}$ ²,

¹ Following classical microlensing conventions, we are taking a maximum source position of $y_{\text{max}} = 1$ as the cross-section threshold. For GWs, the detectability thresholds for y can be different (usually $\gtrsim 1$) than for electromagnetic lensing, and in that case the cross-section is $\pi R_E^2 y_{\text{max}}^2$.

² Throughout this work, due to self-lensing, the distance d_L from the observer to the lens can be taken as practically equal to the distance d_S from the observer to the source.

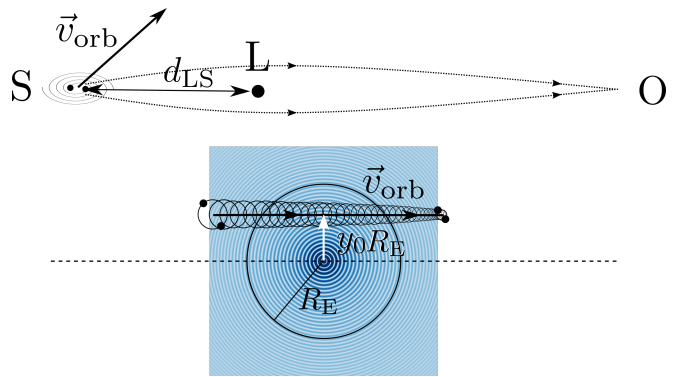


FIG. 1. Schema of the lensing configuration considered in this study. *Top*: The GW source (S) is a compact binary orbiting a MBH at a distance d_{LS} . The MBH acts as a gravitational lens (L), affecting the GW signal, with arrives distorted at the observer (O) when S, L and O are close to alignment. *Bottom*: View from the observer, where the source travels behind the lens. The lensing effect is dominant behind the cross-section of radius R_E and, as we will see in Sec. IV, the amplitude of the signal is modulated by the transmission factor (F in Eq. (3)) shown by the pattern here. The source can have an offset $y_0 R_E$ with respect to the perfect alignment (dashed line going through the center of the lens).

with $R_S = 2GM_{\text{MBH}}/c^2$ being the Schwarzschild radius of the MBH of mass M_{MBH} . G is the gravitational constant and c is the speed of light in vacuum. The source is generally not perfectly aligned (i.e., not crossing exactly behind the lens), it has a physical offset $\eta_0 \simeq y_0 R_E$ where y_0 is the dimensionless source position (“impact parameter”, sometimes known as u_0) of closest approach to the lens at time t_0 . As the source moves, the source position y with respect to the lens changes over time (t),

$$y(t) = \sqrt{y_0^2 + (t - t_0)^2 / t_E^2}, \quad (1)$$

where t_E is the Einstein radius crossing timescale $t_E = R_E / v_{\text{orb}}$.

A. The crossing timescale depends directly on the orbital distance

In self-lensing [44, 47–49], the orbital velocity of the source, if assumed Keplerian and circular, is $v_{\text{orb}} \simeq \sqrt{GM_{\text{MBH}}/d_{LS}}$. The increase in velocity for a larger M_{MBH} is compensated in t_E by a larger cross-section of radius $R_E \simeq \sqrt{2R_S d_{LS}}$, which results on a crossing timescale only dependent on d_{LS} [44]:

$$t_E = \frac{2d_{LS}}{c}. \quad (2)$$

Compared to a general source, this result is not degenerate and provides a direct measure of the distance d_{LS} , as we analyze in the following.

Even in a cosmological situation at a redshift z , the M_{MBH} used in this derivation is the intrinsic mass. Later in the manuscript we will use $M_{\text{MBH},z} \equiv M_{\text{MBH},0}(1+z)$ to represent a redshifted mass.

B. Lensing signature on the GW waveform

In frequency domain, the lensed GW waveform $\tilde{h}(f)$ can be obtained as

$$\tilde{h}(f) = \tilde{h}_{\text{UL}}(f)F(f, y), \quad (3)$$

where $\tilde{h}_{\text{UL}}(f)$ is the unlensed waveform of a GW signal. In general, the transmission factor $F(f, y)$ that imprints the lensing effect depends both on the GW frequency f and on the source position y . When the source is moving, both these variables change over time, $f(t), y(t)$, producing a complex situation.

To obtain the lensed waveform in time domain, $h(t)$, we need to do the inverse Fourier transform of $\tilde{h}(f)$,

$$h(t) = \int df \tilde{h}(f)e^{i2\pi ft} = \int df \tilde{h}_{\text{UL}}(f)F(f, y(t))e^{i2\pi ft}. \quad (4)$$

Our astrophysical situation allows us to use the Geometrical Optics (GO) approximation. For the approximation to be valid, the source position y needs to fulfill the condition [50]

$$y \gtrsim 0.0125 \left(\frac{10 \text{ Hz}}{f} \right) \left(\frac{10^5 M_{\odot}}{M_{\text{MBH},z}} \right), \quad (5)$$

which will be met for the values considered in this study, usually $M_{\text{MBH},z} \gtrsim 10^5 M_{\odot}$, $f \gtrsim 10 \text{ Hz}$.

The GO approximation allows us to simplify Eq. (3) to a sum over different images of magnification $\sqrt{\mu_i}$ each,

$$\tilde{h}(f) = \tilde{h}_{\text{UL}}(f) \sum_{\text{images}(i)} \sqrt{\mu_i} e^{i2\pi ft_i - i\pi n_j/2} \quad (6)$$

$$= \tilde{h}_{\text{UL}}(f) e^{i2\pi ft_1} \left[\sqrt{\mu_1} + \sqrt{\mu_2} e^{i2\pi f\Delta t - i\pi/2} \right], \quad (7)$$

where in the last step we assume the point mass lens, which has two images. Here, t_1 is the arrival time of the first image, and $\Delta t \simeq 4yR_S(1+z)/c$ is the time delay of the second image with respect to the first image, simplified for $y \lesssim 0.5$ [50]. n_j is the topological Morse phase of each image. The GO approximation allows us to split the integral. Furthermore, in GO, the amplitude $|F| = \sqrt{\mu_{1,2}}$ of each image is independent of f , it only depends on y :

$$\sqrt{\mu_{1,2}} = \frac{1}{2} \left(\frac{y}{\sqrt{y^2+4}} + \frac{\sqrt{y^2+4}}{y} \pm 2 \right)^{1/2}. \quad (8)$$

The treatment of the integral gets simpler, because a phase shift in the frequency domain translates to a time shift in time domain.

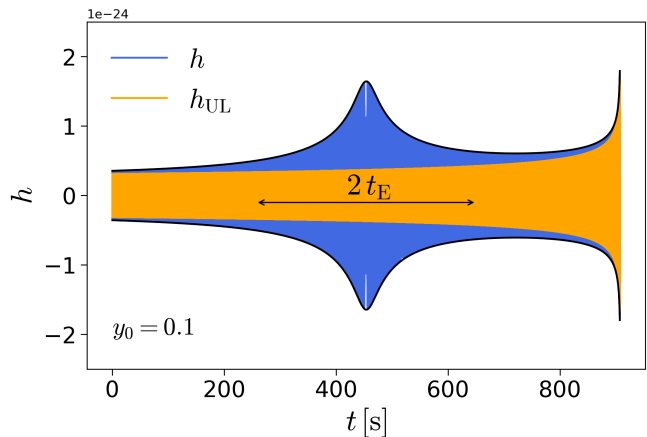


FIG. 2. Representation of a GW signal CBC “chirp”, through the strain h (relative deformation of space-time) as a function of time t . The amplitude of the Paczyński-like curve on the inspiral phase of the signal can be comparable (or even larger) than the final merger. The parameters used here are a source “chirp mass” $M_{\text{chirp}} = 1 M_{\odot}$, a distance from the observer $d_L = 1 \text{ Gpc}$ (just affecting the overall amplitude of the strain), $y_0 = 0.1$ and $d_{\text{LS}} \simeq 3 \times 10^{10} \text{ m}$. In self-lensing, the width of the lensing curve ($2t_E = 4d_{\text{LS}}/c$) is independent on M_{MBH} [Eq. (2)]. Instead, as we will see in Sec. IV, the signal is modulated by an interference pattern, which does depend on M_{MBH} (Fig. 3). For comparison purposes, the lensed signal is represented in the time reference of the arrival time of the first image, t_1 . For simplicity, we represent the inspiral part of the signal from $f \gtrsim 12 \text{ Hz}$, truncated at merger.

The time domain signal is finally described by

$$h(t) = \sqrt{\mu_1} h_{\text{UL}}(t+t_1) + \sqrt{\mu_2} h_{\text{UL}}(t+t_1+\Delta t) e^{-i\pi/2}. \quad (9)$$

Therefore, the signal is a combination of two images of the original source, scaled by a magnification $\sqrt{\mu_{1,2}}$ each and separated by a time delay Δt . For the moving lens, $\sqrt{\mu_{1,2}}$, Δt and t_1 are functions of $y(t)$ [Eq. (1)] and change over time. The difference with the static lens is that Δt changes over time and the contribution from each image reverses as y changes from negative to positive.

A lensed CBC signal is shown in Fig. 2. To interpret it, we start chronologically with the source far from alignment, when the first image looks unlensed ($\sqrt{\mu_1} \rightarrow 1$), the second image is very faint ($\sqrt{\mu_2} \rightarrow 0$) and the time delay between them is large. As the source moves behind the lens, both images are magnified and the time delay becomes shorter. At t_0 , the images arrive simultaneously and at their maximum joint amplification, corresponding to the peak. As the source moves away, the situation is reversed back to the same as in the beginning, in this case the first image gets demagnified until it is too faint ($\sqrt{\mu_1} \rightarrow 0$) and the second image looks unlensed, $\sqrt{\mu_2} \rightarrow 1$.

Although the source waveform $h_{\text{UL}}(t)$ is chosen to be a CBC “chirp”, with frequency dependence $f(t) \propto M_{\text{chirp}}^{-5/8}$, the method can be applied to any smoothly varying

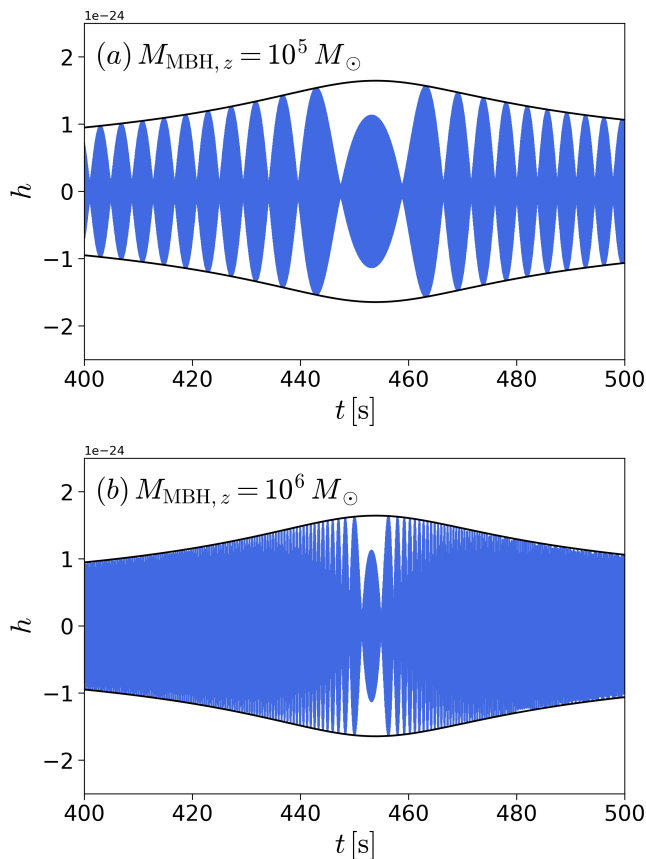


FIG. 3. Zoom-in view of Fig. 2, at the peak of the lensing curve at GW frequencies $f \simeq 15$ Hz. The interference pattern modulating the GW signal depends on the mass, (a) $M_{\text{MBH},z} = 10^5 M_{\odot}$, (b) $M_{\text{MBH},z} = 10^6 M_{\odot}$ and the distance $d_{\text{LS}} \simeq 3 \times 10^{10}$ m (or equivalently $t_{\text{E}} \simeq 200$ s). The modulation period far from the peak can be estimated with Eq. (15), for example here in the segment $t \in (400 - 420)$ s.

source. In Fig. 2, the oscillations are too narrow to distinguish the interference pattern or the phase. A zoom view is seen in Fig. 3: while the interference pattern modulations are distinguished, the oscillations still have too many cycles to be resolved by eye. In this work, the amplitude already gives us enough information. However, the phase may give additional information about environmental phase shifts, which are not taken into account here and may be required in more exhaustive searches.

In ground-based GW detectors, this lensing curve on the GW signal may appear as an excess power. If not taken into account, the full signal may be missed or misinterpreted. Although in most cases it might not be confused with short bursts (glitches or other burst signals such as eccentric pulses/bursts [51]) because t_{E} is generally longer than their duration, the lensing curve should be taken into account when treating multiple overlapping signals in next-generation detectors.

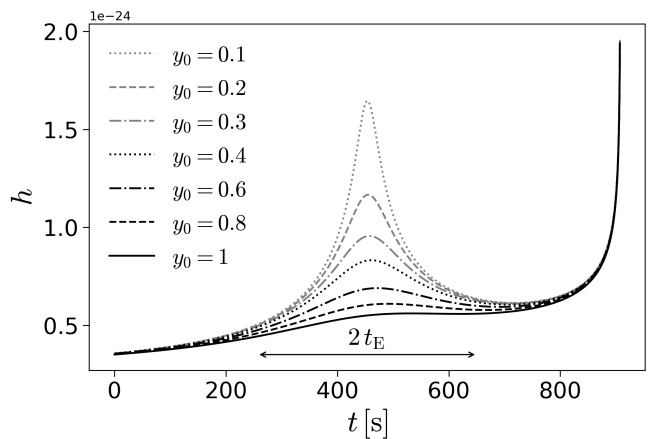


FIG. 4. Amplitude of the signal (envelope curve) as a function of the closest source position y_0 . The curve follows a Paczyński-like curve. The width of the curve is $2t_{\text{E}}$: it is practically independent on y_0 , and for self-lensing it only depends on d_{LS} [Eq. (2)].

III. OBTAINING THE ORBITAL DISTANCE

The envelope of the lensing signature follows a Paczyński-like curve [22] in the part of the inspiral where the source passes behind the lens. By contrast to the optical microlensing curve, given by multiplying the signal by the amplification $\mu_1 + \mu_2 = (y^2 + 2)/(y\sqrt{y^2 + 4})$ [22], the GW lensing curve depends on $\sqrt{\mu_1}$ and $\sqrt{\mu_2}$ multiplying each of the time-dependent images.

The width of the curve is given by $2t_{\text{E}}$. Figure 4 shows that this width is practically independent on y_0 . Therefore, the distance d_{LS} can then directly be obtained by measuring the crossing time $2t_{\text{E}}$ [Eq. (2)]:

$$d_{\text{LS}} \simeq 1.5 \times 10^{10} \text{ m} \left(\frac{t_{\text{E}}}{100 \text{ s}} \right). \quad (10)$$

The prospects for observability depend on the astrophysical nature of the sources that can emit light or GWs:

Observability for sources of light. The light-curve may be seen for long timescales, provided that the source is at a distance d_{LS} larger than the tidal disruption radius of the source R_{tidal} . For typical R_{tidal} of stars around MBHs, we can expect $t_{\text{E}} \gtrsim 3$ hours. Low mass MBHs may be favored due to their potential to produce short timescales because $d_{\text{LS}} > R_{\text{tidal}} \propto M_{\text{MBH}}^{1/3}$, which can be interesting for the MBH at the center of our Galaxy (expanded in the Discussion, VI) or intermediate-mass black holes (IMBHs) at the centers of star clusters.

Observability for GW signals. The full lensing curve can be seen when $2t_{\text{E}} < t_{\text{insp}}$, where t_{insp} is the

inspiral time given by [52]

$$t_{\text{insp}} = \frac{5}{256} (\pi f_{\text{th}})^{-8/3} \left(\frac{GM_{\text{chirp}}}{c^3} \right)^{-5/3} \quad (11)$$

$$\sim 10^3 \text{ s} \left(\frac{10 \text{ Hz}}{f_{\text{th}}} \right)^{8/3} \left(\frac{1 M_{\odot}}{M_{\text{chirp}}} \right)^{5/3}. \quad (12)$$

Here M_{chirp} is the ‘‘chirp mass’’ of the source, and f_{th} is the threshold frequency from where the signal starts to be detectable, which one may take $f_{\text{th}} \sim 10 \text{ Hz}$. The condition $2t_{\text{E}} < t_{\text{insp}}$ leads to

$$d_{\text{LS}} \lesssim 10^{11} \text{ m} \left(\frac{1 M_{\odot}}{M_{\text{chirp}}} \right)^{5/3}. \quad (13)$$

Otherwise, only part of the curve is observable.

Such close distances may be reached in active galactic nuclei (AGN) disks, if the sources are in migration traps [53–55]. For example, fixing the distance at $d_{\text{LS}} \sim 10 R_{\text{S}}$ [56, 57], for $M_{\text{chirp}} = 1 M_{\odot}$, a complete curve appears for $M_{\text{MBH},z} \lesssim 3 \cdot 10^6 M_{\odot}$.

IV. OBTAINING THE MBH MASS

The lensed GW signal presents a modulation of the amplitude which can be seen in Fig. 3 (a zoom-in view of Fig. 2). The modulation is caused by the phase difference between the lensed images, which creates an interference pattern that can also be found in continuous GW signals [31]. The period of this modulation can be roughly estimated in the GO approximation from Eq. (7), $T = t/(f\Delta t)$ [58], using $y \sim t/t_{\text{E}}$. This period is only formally valid for the radial spacing (interference pattern in Fig. 1). Since in our case the source has an offset y_0 , the period will asymptotically match the modulations far from the t_0 peak. Nevertheless, the point of this estimation is to show that the period is inversely proportional to the mass of the MBH,

$$T \simeq \frac{d_{\text{LS}}}{2R_{\text{S}}} \frac{1}{1+z} \left(\frac{1}{f} \right) \quad (14)$$

$$\simeq 2.5 \text{ s} \left(\frac{t_{\text{E}}}{100 \text{ s}} \right) \left(\frac{10^5 M_{\odot}}{M_{\text{MBH},z}} \right) \left(\frac{10 \text{ Hz}}{f} \right). \quad (15)$$

By observing the modulation period T and the GW frequency f ³, we can obtain the mass of the MBH:

$$M_{\text{MBH},z} \simeq 2.5 \times 10^6 M_{\odot} \left(\frac{t_{\text{E}}}{100 \text{ s}} \right) \frac{1}{fT}. \quad (16)$$

For the astrophysical parameters we consider (typical MBH masses and LVK/ET/CE frequencies), these modulations are expected to last $\gtrsim \text{s}$. The interference pattern is thus potentially resolvable in time domain in current ground-based GW detectors.

³ The frequency is assumed to be directly measurable by the detector from the incoming GWs.

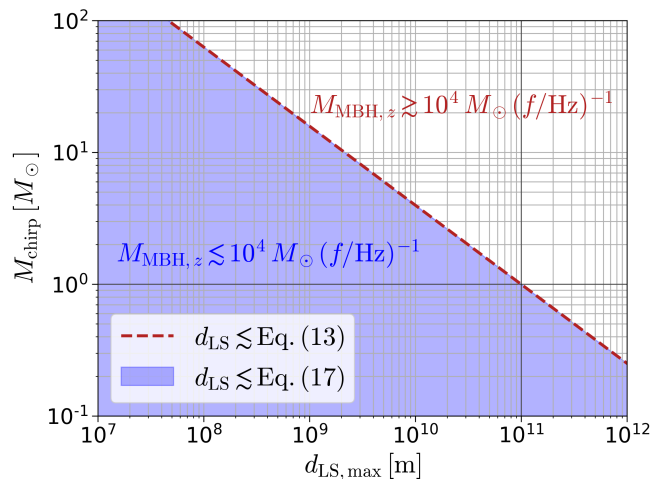


FIG. 5. Parameter thresholds to detect d_{LS} and $M_{\text{MBH},z}$ jointly. If $M_{\text{MBH},z} \gtrsim 10^4 M_{\odot} (\text{Hz}/f)$, the maximum distance d_{LS} given a value of M_{chirp} is limited by observing t_{E} , shown by the red dashed line (Eq. (13)). If $M_{\text{MBH},z} \lesssim 10^4 M_{\odot} (\text{Hz}/f)$, the threshold lies in the blue region, where the exact curve depends on the different parameters in Eq. (17).

The condition to observe at least a few of these modulations is that the period has to be shorter than the duration of the signal, $T < t_{\text{insp}}$, leading to

$$d_{\text{LS}} \lesssim 2 \times 10^4 R_{\text{S}}(1+z) \left(\frac{f}{10 \text{ Hz}} \right) \left(\frac{1 M_{\odot}}{M_{\text{chirp}}} \right)^{5/3}. \quad (17)$$

These distances might be reached in AGN disks, where compact binaries may orbit in migration traps at $d_{\text{LS}} \sim (10 - 10^3) R_{\text{S}}$ [54–56, 59, 60].

A. Joint observation of d_{LS} and $M_{\text{MBH},z}$

To obtain $M_{\text{MBH},z}$ we require knowing t_{E} (from the width of the curve) and observing the modulations. For that, d_{LS} has to fulfill the two conditions in Eqs. (13) and (17). For a mass above

$$M_{\text{MBH},z} = 10^4 M_{\odot} \left(\frac{\text{Hz}}{f} \right), \quad (18)$$

the limitation comes from being able to obtain d_{LS} from the crossing timescale, Eq. (13), shown in a red dashed line in Fig. 5. For a lower $M_{\text{MBH},z}$ than Eq. (18), the limitation comes from being able to see at least a few modulations, Eq. (17), in the blue region in Fig. 5. For this latter case, the exact limiting curve depends on the various parameters in Eq. (17), and in general it is more restrictive on the maximum value of d_{LS} than Eq. (13).

From those joint constraints, we conclude that the threshold distances $d_{\text{LS,max}}$ lie within observational ranges, comparing them to Schwarzschild radii values

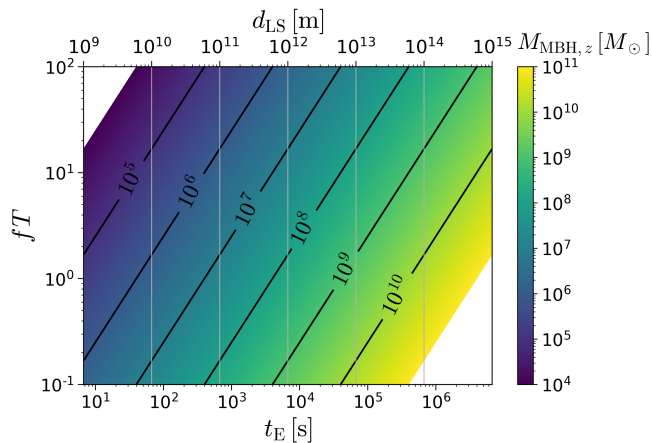


FIG. 6. Summary of the relations between parameters and how to obtain d_{LS} and $M_{\text{MBH},z}$ from measuring t_{E} , f and T . By measuring t_{E} from the width of the curve, we obtain d_{LS} through Eq. (2). In GWs, the interference pattern can provide information about the modulation period T . By observing T , the GW frequency f and t_{E} , we can estimate $M_{\text{MBH},z}$ with Eq. (16).

of $R_{\text{S}} \simeq 3 \times 10^9 \text{ m}$ ($M_{\text{MBH}}/[10^6 M_{\odot}]$). Therefore, it is possible to measure both d_{LS} and $M_{\text{MBH},z}$ in realistic astrophysical scenarios, especially in AGN disks. Figure 6 summarizes how to obtain simultaneously d_{LS} and $M_{\text{MBH},z}$ once f , T and t_{E} can be measured from the GW signal.

The expected MBH masses and distance distributions depend on the astrophysical environment (star clusters, galactic nuclei, AGN disks) and its formation channels for GW sources. Measuring d_{LS} and $M_{\text{MBH},z}$ from the same signal may help distinguish the environment where the GW signal comes from, by comparing them to the expected values of d_{LS} and $M_{\text{MBH},z}$ for each environment.

V. INFERRING THE ORBITAL INCLINATION OF THE BINARY

It may be possible to infer the inclination of the orbit θ with respect to the line of sight if the distance d_{LS} , the MBH mass M_{MBH} , and y_0 ⁴ can be obtained from the signal. Given that $y_0 \simeq \eta_0/R_{\text{E}}$ is the normalization of the physical offset η_0 in self-lensing, and the inclination angle of the orbit with respect to the line of sight is given by $\theta \approx \eta_0/d_{\text{LS}}$ for small angles, the inclination can be estimated as

$$\theta \approx y_0 R_{\text{E}}/d_{\text{LS}} \quad (19)$$

$$\simeq 14^\circ y_0 \left(\frac{M_{\text{MBH}}}{10^6 M_{\odot}} \right)^{1/2} \left(\frac{10^{11} \text{ m}}{d_{\text{LS}}} \right)^{1/2}. \quad (20)$$

⁴ The value of y_0 can be estimated from the relative amplitude of the curve, see Fig. 4.

Knowing about the inclination of orbiting compact binaries can be interesting especially in AGN disk environments, which is an area of active study [61].

VI. DISCUSSION

The prospects of observing the lensing Paczyński-like curve depend on the probability that the source is emitting the GW signal when it moves behind the lens. The probability of having self-lensing of a static source can reach $\sim 1\%$, for example in AGN disks [46, 57, 62]. Given that a moving source covers a larger region than a static source during the emission of the signal, it is expected that the probability is equal or higher than the static self-lensing case. More work is needed to quantify it.

Wave effects appear here as the interference of the multiple images. The GO approximation holds for large masses, although the complete wave optics formalism may need to be considered for low masses (for example, IMBHs in star clusters) or very closely aligned orbits $y_0 \rightarrow 0$ [e.g., 31] when condition (5) is not met. In this case, if the integral in Eq. (4) has a transmission factor that depends on both $f(t)$ and $y(t)$ (for example, in the point mass, the product fy appears as a variable), it probably becomes more complex to solve.

We have focused on the amplitude of the signal for this study, without entering into details of the phase. There is a global shift in Eq. (7) given by the time dependence of the absolute time of arrival t_1 of the first image. This would need to be carefully modeled, especially if environmental effects that cause phase shifts [63] are taken into account. Precisely, Doppler shifts, gravitational redshift, beaming and strong gravity effects in general [64] may become important at very short d_{LS} ($\sim R_{\text{S}}$). We do not take them into account in this work, and also neglect the effect of the Earth's rotation on the amplitude.

Additionally, environmental effects may distort the signal or modify its inspiral time. Further work is required to evaluate the potential degeneracies of these effects and disentangle them.

For this work we have assumed a circular orbit. For an elliptical orbit, d_{LS} should be replaced by a , the semi-major axis: $v_{\text{orb}} = \sqrt{GM_{\text{MBH}}/a}$. In this case, the eccentricity of the orbit might reintroduce a degeneracy in t_{E} .

Although we quantified the maximum d_{LS} , some sources are limited by a minimum d_{LS} as well. For example, stars below $d_{\text{LS}} < R_{\text{tidal}}$ are tidally disrupted, which reduces the probability of observing the optical Paczyński light-curve for large M_{MBH} systems. For low MBH masses, however, they may still be detectable: for our Galaxy's central MBH, light-curves from orbiting stars may last for $2t_{\text{E}} \gtrsim 8$ hours. However, currently known stars from the S-star cluster are further away, and not very likely to be microlensed by the MBH [65], requiring very powerful telescopes [66].

VII. CONCLUSIONS

The geometrical configuration in self-lensing breaks the usually found microlensing degeneracy for the Einstein crossing timescale t_E . It is therefore possible to extract the properties of the system from the lensing signature:

- For both light and GW sources, the orbital distance d_{LS} of the source can be obtained from the measure of the crossing timescale t_E (half width of the curve), $d_{LS} \simeq 1.5 \times 10^{10} \text{ m} (t_E/[100 \text{ s}])$ [Eq. (10)]. For GW sources, the full curve may be observed for $d_{LS} \lesssim 10^{11} \text{ m} (1 M_\odot/M_{\text{chirp}})^{5/3}$. Short timescales are favored in systems with low M_{MBH} , which allow smaller values of d_{LS} . For light, the light-curve can be observed for as long as the observation time.
- The mass $M_{\text{MBH},z}$ of the MBH lens can be obtained from the interference pattern in GW signals. Given the modulation period T , the instantaneous GW frequency f , and t_E , $M_{\text{MBH},z} \simeq 2.5 \times 10^6 M_\odot (t_E/[100 \text{ s}]) (f T)^{-1}$ [Eq. (16)]. These modulations are expected to be visible typically for $d_{LS} \lesssim 10^4 R_S (1 M_\odot/M_{\text{chirp}})^{5/3}$. However, to measure $M_{\text{MBH},z}$, both conditions in Eq. (13) and (17) should be met. Figure 6 summarizes how to obtain simultaneously d_{LS} and $M_{\text{MBH},z}$ by observing f , T and t_E . We conclude that $M_{\text{MBH},z}$ can be realistically obtained in astrophysical environments through self-lensing. The mass measurement can be extended to other GW signals such as continuous GWs.

Self-lensing therefore offers a complementary way to obtain d_{LS} and $M_{\text{MBH},z}$ additionally to the simultaneous measure of the velocity and acceleration presented in [45].

- If the distance d_{LS} , the mass M_{MBH} and y_0 could be simultaneously obtained in GWs, it would be

possible to infer the inclination of orbit with respect to the line of sight, $\theta \propto y_0 M_{\text{MBH}}^{1/2} d_{LS}^{-1/2}$ [Eq. (20)].

Obtaining d_{LS} and $M_{\text{MBH},z}$ simultaneously would provide valuable information about the environment of the binary [e.g., 45]. Consequently, it would help constrain the astrophysical environments where GW signals come from.

ACKNOWLEDGEMENTS

This work has been inspired by conversations about moving sources with Sudhagar Suyamprakasam, Mikolaj Korzyński and Sreekanth Harikumar at the workshop “Lensing and Wave Optics in Strong Gravity” at the Erwin Schrödinger International Institute for Mathematics and Physics (ESI). I would like to thank the organizers of the workshop and its participants for such an inspiring atmosphere. I am grateful to Johan Samsing for engaging discussions later at the Niels Bohr Institute, and I would like to thank him and Lorenz Zwick for useful comments on early results of this work. I am deeply grateful for the hospitality of all colleagues at the Niels Bohr Institute, where part of this work was carried out. I would like to thank Mark Gieles and Jordi Miralda Escudé for providing useful feedback on the draft and for very insightful comments.

Software: All the presented results are analytical, and the corresponding figures have been produced with Python (Numpy, Matplotlib). Fig. 1 has been created with Inkscape. I declare that this work has been developed without use of artificial intelligence.

Financial support: FI-SDUR 2023 predoctoral grant (AGAUR, Generalitat de Catalunya), which also covered the visit to the Niels Bohr Institute. PID2024-159689NB-C22, CEX2024-001451-M funded by MCIN/AEI/10.13039/501100011033, and SGR-2021-01069 (AGAUR, Generalitat de Catalunya).

-
- [1] D. Walsh, R. F. Carswell, and R. J. Weymann, *Nature* **279**, 381 (1979).
 - [2] C. Alcock, C. W. Akerlof, R. A. Allsman, T. S. Axelrod, D. P. Bennett, S. Chan, K. H. Cook, K. C. Freeman, K. Griest, S. L. Marshall, H.-S. Park, S. Perlmutter, B. A. Peterson, M. R. Pratt, P. J. Quinn, A. W. Rodgers, C. W. Stubbs, and W. Sutherland, *Nature* **365**, 621 (1993), [arXiv:astro-ph/9309052 \[astro-ph\]](#).
 - [3] A. Udalski, M. Szymanski, J. Kaluzny, M. Kuibak, W. Krzeminski, M. Mateo, G. W. Preston, and B. Paczynski, *Acta Astron.* **43**, 289 (1993).
 - [4] O. A. Hannuksela, K. Haris, K. K. Y. Ng, S. Kumar, A. K. Mehta, D. Keitel, T. G. F. Li, and P. Ajith, *ApJ* **874**, L2 (2019), [arXiv:1901.02674 \[gr-qc\]](#).
 - [5] L. Dai, B. Zackay, T. Venumadhav, J. Roulet, and M. Zaldarriaga, [arXiv e-prints](#), [arXiv:2007.12709 \(2020\)](#), [arXiv:2007.12709 \[astro-ph.HE\]](#).
 - [6] LIGO Scientific Collaboration and Virgo Collaboration, *ApJ* **923**, 14 (2021), [arXiv:2105.06384 \[gr-qc\]](#).
 - [7] The LIGO Scientific Collaboration, the Virgo Collaboration, and the KAGRA Collaboration, [arXiv e-prints](#), [arXiv:2304.08393 \(2023\)](#), [arXiv:2304.08393 \[gr-qc\]](#).
 - [8] J. Janquart, M. Wright, S. Goyal, J. C. L. Chan, A. Ganguly, Á. Garrón, D. Keitel, A. K. Y. Li, A. Liu, R. K. L. Lo, A. Mishra, A. More, H. Phurailatpam, P. Prasia, P. Ajith, S. Biscoveanu, P. Cremonese, J. R. Cudell, J. M. Ezquiaga, J. Garcia-Bellido, O. A. Hannuksela, K. Haris, I. Harry, M. Hendry, S. Husa, S. Kapadia, T. G. F. Li, I. Magaña Hernandez, S. Mukherjee, E. Seo, C. Van Den Broeck, and J. Veitch, *MNRAS* **526**, 3832 (2023), [arXiv:2306.03827 \[gr-qc\]](#).
 - [9] The LIGO Scientific Collaboration, the Virgo Collaboration, and the KAGRA Collaboration, [arXiv e-prints](#), [arXiv:2507.08219 \(2025\)](#), [arXiv:2507.08219 \[astro-ph\]](#).

- ph.HE].
- [10] B. P. Abbott *et al.*, *Physical Review X* **9**, 031040 (2019), arXiv:1811.12907 [astro-ph.HE].
- [11] R. Abbott *et al.*, *Physical Review X* **11**, 021053 (2021), arXiv:2010.14527 [gr-qc].
- [12] R. Abbott *et al.*, *Physical Review X* **13**, 041039 (2023), arXiv:2111.03606 [gr-qc].
- [13] T. Venumadhav, B. Zackay, J. Roulet, L. Dai, and M. Zaldarriaga, *Phys. Rev. D* **101**, 083030 (2020), arXiv:1904.07214 [astro-ph.HE].
- [14] B. Zackay, L. Dai, T. Venumadhav, J. Roulet, and M. Zaldarriaga, *Phys. Rev. D* **104**, 063030 (2021), arXiv:1910.09528 [astro-ph.HE].
- [15] The LIGO Scientific Collaboration, The Virgo Collaboration, and the KAGRA Collaboration, arXiv e-prints , arXiv:2508.18082 (2025), arXiv:2508.18082 [gr-qc].
- [16] K. K. Y. Ng, K. W. K. Wong, T. Broadhurst, and T. G. F. Li, *Phys. Rev. D* **97**, 023012 (2018), arXiv:1703.06319 [astro-ph.CO].
- [17] S.-S. Li, S. Mao, Y. Zhao, and Y. Lu, *MNRAS* **476**, 2220 (2018), arXiv:1802.05089 [astro-ph.CO].
- [18] M. Oguri, *MNRAS* **480**, 3842 (2018), arXiv:1807.02584 [astro-ph.CO].
- [19] F. Xu, J. M. Ezquiaga, and D. E. Holz, *ApJ* **929**, 9 (2022), arXiv:2105.14390 [astro-ph.CO].
- [20] S. Mukherjee, T. Broadhurst, J. M. Diego, J. Silk, and G. F. Smoot, *MNRAS* **506**, 3751 (2021), arXiv:2106.00392 [gr-qc].
- [21] A. R. A. C. Wierda, E. Wempe, O. A. Hannuksela, L. V. E. Koopmans, and C. Van Den Broeck, *ApJ* **921**, 154 (2021), arXiv:2106.06303 [astro-ph.HE].
- [22] B. Paczynski, *ApJ* **304**, 1 (1986).
- [23] T. T. Nakamura, *Phys. Rev. Lett.* **80**, 1138 (1998).
- [24] R. Takahashi and T. Nakamura, *ApJ* **595**, 1039 (2003), arXiv:astro-ph/0305055 [astro-ph].
- [25] K. Liao, M. Biesiada, and X.-L. Fan, *ApJ* **875**, 139 (2019), arXiv:1903.06612 [gr-qc].
- [26] D. Sun and X. Fan, arXiv e-prints , arXiv:1911.08268 (2019), arXiv:1911.08268 [gr-qc].
- [27] S. Hou, X.-L. Fan, K. Liao, and Z.-H. Zhu, *Phys. Rev. D* **101**, 064011 (2020), arXiv:1911.02798 [gr-qc].
- [28] M. Biesiada and S. Harikumar, *Universe* **7**, 502 (2021), arXiv:2111.05963 [gr-qc].
- [29] F. De Paolis, G. Ingrosso, and A. A. Nucita, *A&A* **366**, 1065 (2001), arXiv:astro-ph/0011563 [astro-ph].
- [30] X. Guo and Z. Cao, *J. Cosmology Astropart. Phys.* **2024**, 084 (2024), arXiv:2401.01581 [astro-ph.HE].
- [31] S. Suyamprakasam, S. Harikumar, P. Ciecielag, P. Figura, M. Bejger, and M. Biesiada, arXiv e-prints , arXiv:2503.21845 (2025), arXiv:2503.21845 [gr-qc].
- [32] X.-Y. Yang, T. Chen, and R.-G. Cai, *J. Cosmology Astropart. Phys.* **2025**, 069 (2025), arXiv:2410.16378 [astro-ph.CO].
- [33] Y.-Z. Li, W.-L. Xu, Y.-G. Chen, and W.-H. Lei, arXiv e-prints , arXiv:2506.04196 (2025), arXiv:2506.04196 [astro-ph.HE].
- [34] D. J. D’Orazio and A. Loeb, *Phys. Rev. D* **101**, 083031 (2020), arXiv:1910.02966 [astro-ph.HE].
- [35] H. Yu, Y. Wang, B. Seymour, and Y. Chen, *Phys. Rev. D* **104**, 103011 (2021), arXiv:2107.14318 [gr-qc].
- [36] S. Refsdal, *MNRAS* **134**, 315 (1966).
- [37] A. Gould, *ApJ* **421**, L75 (1994).
- [38] A. Gould, *ApJ* **542**, 785 (2000), arXiv:astro-ph/0001421 [astro-ph].
- [39] C.-H. Lee, *Universe* **3**, 53 (2017), arXiv:1711.05298 [astro-ph.IM].
- [40] A. Gould, *Journal of Korean Astronomical Society* **52**, 121 (2019), arXiv:1905.06770 [astro-ph.EP].
- [41] A. Gould, *ApJ* **421**, L71 (1994).
- [42] R. J. Nemiroff and W. A. D. T. Wickramasinghe, *ApJ* **424**, L21 (1994), arXiv:astro-ph/9401005 [astro-ph].
- [43] S. Rahvar, *Phys. Rev. D* **101**, 024015 (2020), arXiv:1908.01361 [astro-ph.GA].
- [44] S. Rahvar, A. Mehrabi, and M. Dominik, *MNRAS* **410**, 912 (2011), arXiv:1008.1033 [astro-ph.SR].
- [45] J. Samsing, L. Zwick, P. Saini, and J. Takátsy, arXiv e-prints , arXiv:2511.19407 (2025), arXiv:2511.19407 [astro-ph.HE].
- [46] H. Ubach, M. Gieles, and J. Miralda-Escudé, *Phys. Rev. D* **112**, 083026 (2025), arXiv:2505.04794 [astro-ph.HE].
- [47] G. M. Beskin and A. V. Tuntsov, *A&A* **394**, 489 (2002), arXiv:astro-ph/0208095 [astro-ph].
- [48] S. Kasuya, M. Honda, and R. Mishima, *MNRAS* **411**, 1863 (2011), arXiv:1009.2129 [astro-ph.EP].
- [49] C. Han, *ApJ* **820**, 53 (2016), arXiv:1603.03500 [astro-ph.SR].
- [50] O. Bulashenko and H. Ubach, *J. Cosmology Astropart. Phys.* **2022**, 022 (2022), arXiv:2112.10773 [gr-qc].
- [51] J. Samsing, K. Hendriks, L. Zwick, D. J. D’Orazio, and B. Liu, *ApJ* **990**, 211 (2025), arXiv:2403.05625 [astro-ph.HE].
- [52] M. Maggiore, *Gravitational Waves: Volume 1: Theory and Experiments* (Oxford University Press, 2007).
- [53] B. McKernan, K. E. S. Ford, W. Lyra, and H. B. Perets, *MNRAS* **425**, 460 (2012), arXiv:1206.2309 [astro-ph.GA].
- [54] J. M. Bellovary, M.-M. Mac Low, B. McKernan, and K. E. S. Ford, *ApJ* **819**, L17 (2016), arXiv:1511.00005 [astro-ph.GA].
- [55] A. Secunda, J. Bellovary, M.-M. Mac Low, K. E. S. Ford, B. McKernan, N. W. C. Leigh, W. Lyra, and Z. Sándor, *ApJ* **878**, 85 (2019).
- [56] P. Peng and X. Chen, *MNRAS* **505**, 1324 (2021), arXiv:2104.07685 [astro-ph.HE].
- [57] S. H. W. Leong, J. Janquart, A. K. Sharma, P. Martens, P. Ajith, and O. A. Hannuksela, *ApJ* **979**, L27 (2025), arXiv:2408.13144 [astro-ph.HE].
- [58] S. Savastano, F. Vernizzi, and M. Zumalacárregui, *Phys. Rev. D* **109**, 024064 (2024), arXiv:2212.14697 [gr-qc].
- [59] D. Gangardt, A. A. Trani, C. Bonnerot, and D. Gerosa, *MNRAS* **530**, 3689 (2024), arXiv:2403.00060 [astro-ph.HE].
- [60] E. Grishin, S. Gilbaum, and N. C. Stone, *MNRAS* **530**, 2114 (2024), arXiv:2307.07546 [astro-ph.HE].
- [61] C. Rowan, H. Whitehead, G. Fabj, P. Kirkeberg, M. E. Pessah, and B. Kocsis, *MNRAS* **543**, 132 (2025), arXiv:2505.23739 [astro-ph.HE].
- [62] L. Gondán and B. Kocsis, *MNRAS* **515**, 3299 (2022), arXiv:2110.09540 [astro-ph.HE].
- [63] J. Takátsy, L. Zwick, K. Hendriks, P. Saini, G. Fabj, and J. Samsing, *Classical and Quantum Gravity* **42**, 215006 (2025), arXiv:2505.09513 [astro-ph.HE].
- [64] J. S. Santos, V. Cardoso, J. Natário, and M. van de Meent, *Phys. Rev. Lett.* **135**, 211402 (2025), arXiv:2506.14868 [gr-qc].
- [65] M. J. Michałowski and P. Mróz, *ApJ* **915**, L33 (2021),

[arXiv:2107.00659](#) [astro-ph.GA].

[66] V. Bozza and L. Mancini, *ApJ* **753**, 56 (2012),
[arXiv:1204.2103](#) [astro-ph.GA].